Biosensors and Bioelectronics 100 (2018) 396–403

Contents lists available at ScienceDirect

Biosensors and Bioelectronics

journal homepage: www.elsevier.com/locate/bios

Development of a bifunctional nanobiosensor for screening and detection of chemokine ligand in colorectal cancer cell line

Saeromi Chung[a], Pranjal Chandra[b], Jaseok Peter Koo[c], Yoon-Bo Shim[a,*]

[a] Department of Chemistry and Institute of BioPhysio Sensor Technology (IBST), Pusan National University, Busan 609-735, South Korea
[b] Department of Biosciences and Bioengineering, Indian Institute of Technology Guwahati, Guwahati 781039, Assam, India
[c] Department of Internal Medicine, Yale Cancer Center, Yale School of Medicine, 333 Cedar Street, New Haven, CT 06520, USA

ARTICLE INFO

Keywords:
Human Health
Bifunctional nanobiosensor
Chemokine
Cancer, Colorectal cancer cells
In vitro diagnosis
Human serum

ABSTRACT

Highly sensitive detection of chemokines in various biological matrices and its interaction with a natural receptor molecule has tremendous importance in cell signaling, medical diagnostics, and therapeutics. In this direction, we have designed the first bifunctional nanobiosensor for chemokine screening and detection in a single experimental setting. The sensor probe was fabricated by immobilizing CXCR2 on the gold nanoparticles (AuNPs) deposited 2,2′:5′,2"-terthiophene-3′ (p-benzoic acid) (TBA) nanocomposite film. The interaction between CXCR2 and chemokines was studied using electrochemical impedance spectroscopy (EIS) and voltammetry. CXCL5 among three ligands showed the strongest affinity to CXCR2, which was further utilized to develop an amperometric CXCL5 biosensor. Analytical parameters, such as CXCR2 receptor concentration, temperature, pH, and incubation time were optimized to obtain the high sensitivity. A dynamic range for CXCL5 detection was obtained between 0.1 and 10 ng/mL with the detection limit of 0.078 ± 0.004 ng/mL (RSD < 4.7%). The proposed biosensor was successfully applied to detect CXCL5 in clinically relevant concentrations in human serum and colorectal cancer cells samples with high sensitivity and selectivity. Interference effect and the stability of the developed biosensor were also evaluated. Method verification was performed by comparing the results using commercially available ELISA kit for CXCL5 detection.

1. Introduction

Chemokines are a family of small cytokines or signaling proteins secreted by cells (Le et al., 2004). They have tremendous importance in cell signaling, diagnostics, and therapeutics (Cyster, 1999). It has been reported that chemokine ligands (CXCLs) levels are elevated in various tumors isolated from cancer patient's tissue samples (Bersini et al., 2014). The role of CXCL expression is also directly correlated with tumor growth, tumor derived angiogenesis, and metastasis (Balkwill, 2004; Bersini et al., 2014). The interaction of various CXCLs (eg: CXCL5, CXCL8, CXCL13) with the natural receptor molecule is very important, and possess various biological functions (Sun et al., 2008), even though no comparative binding study between ligands and receptor has been done till date. Among all the CXCLs, CXCL5 has been extensively studied over the years and it has been identified as a novel prognostic factor in various cancers (Ben-Baruch, 2012; Sun et al., 2008; Kowalczuk et al., 2014). Therefore, CXCL5 is a valuable biomarker to study the prognosis of various cancer which may provide valuable information's to clinicians, eventually helpful in cancer therapy. In view of such an important clinical biomarker, CXCL5 or its expression levels has been analyzed using enzyme-linked immunosorbent assay (Agarwal et al., 2013), immunohistochemistry (Kawamura et al., 2012), and quantitative real-time PCR (Li et al., 2011) in various biological samples. These methods are important; however, they have limited point-of-care clinical applications because they are lengthy, require highly trained professionals, and in ability of point-of-care analysis. Thus, the development of a sensitive, robust, and alternate method for CXCL5 detection in the clinically relevant range in body fluids as well as cancer cell model is extremely important and clinically significant, which may provide valuable information's to clinicians to understand cancer progression, eventually assisting in cancer therapy. To do this, an electrochemical biosensor can be preferred over other detection methods due to its robustness, user friendly mode of operation, and ability of miniaturization for on-site medical diagnosis (Rahman et al., 2008; Hussain et al., 2017). It is worthwhile to indicate here that in this work we aim to design a bifunctional electrochemical biosensor which can perform dual task in a single experimental design. First, finding the best ligand (CXCL5) for its interaction with the natural receptor and second quantitative detection of CXCL5 in human serum and cancer cell model to show its clinical

* Corresponding author.
E-mail address: ybshim@pusan.ac.kr (Y.-B. Shim).

http://dx.doi.org/10.1016/j.bios.2017.09.031
Received 18 July 2017; Received in revised form 13 September 2017; Accepted 18 September 2017
Available online 20 September 2017

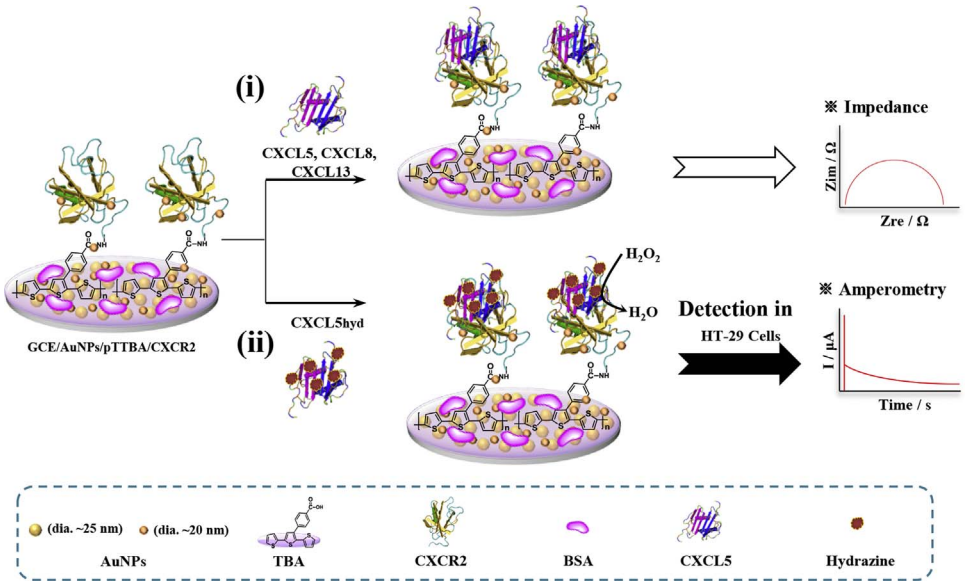

Scheme 1. Schematic diagram of the bifunctional CXCR2 sensor probe for (i) chemokine selection and (ii) CXCL5 detection in human serum and colorectal cancer cells.

importance.

Among various bioreceptors for CXCL5 detection, a chemokine receptor molecule "CXCR2", having natural affinity (Thomson and Lotze, 2003) would be interesting to attempt, which may offer high binding affinity, eventually assisting in highly sensitive CXCL5 biosensor development. We have experimentally observed that CXCL5 has the highest affinity to CXCR2 sensor probe than CXCL8 and CXCL13. To achieve a highly sensitive detection of CXCL5, chronoamperometry based nanobiosensor is worthy to attempt due to its high selectivity, stability, and sensitivity (Bardea et al., 1999; Chandra, 2016; Zhu et al., 2012). To do this, the stable immobilization of bioreceptors on the sensor probe surface is very important and critical in biosensor fabrication (Chandra et al., 2011; Kwon et al., 2006; Lee and Shim, 2001). Electrochemical biosensors fabricated using conducting polymers-AuNPs composite (Koh et al., 2011; Kim and Shim, 2013; Chandra et al., 2015) are known to be highly stable and ultrasensitive because the receptor biomolecules can be covalently immobilized on the polymer backbone comprising -COOH or -NH_2 groups (Lee and Shim, 2001; Rahman et al., 2004; Kim et al., 2009).

In the present study, we have systematically studied the interaction between a chemokine receptor and chemokines using a bifunctional nanobiosensor. The fabricated biosensor was characterized by various methods. The experimental parameters were optimized and the detection limit of a target chemokine ligand was determined. The developed sensor was operated in amperometric format to detect CXCL5 directly in human serum and colorectal cancer cells for the first time to show its real clinical value. The selectivity of the biosensor was also examined toward various non-target proteins and biochemicals present in the real sample matrix. The sensing results were also validated by comparing them with commercial ELISA.

2. Experimental

2.1. Materials

2,2′:5′,2"-terthiophene-3′ (p-benzoic acid) (TBA) was synthesized using the Paal-Knorr pyrrole condensation reaction (Kim et al., 2009). Tetrabutylammonium perchlorate (TBAP, electrochemical grade) was purchased from Fluka (USA) and purified according to a general laboratory method followed by drying under vacuum at 1.33×10^{-3} Pa. CXCR2 receptor, CXCL5, CXCL8, CXCL13 ligands were purchased from Abcam (USA). 1-Ethyl-3-(3-dimethylamino-propyl) carbodiimide (EDC), *N*-hydroxysuccinimide (NHS), gold(III) chloride trihydrate ($HAuCl_4 \cdot 3H_2O$), dichloromethane (99.8%, anhydrous, and sealed under N_2 gas), sodium citrate ($C_6H_5Na_3O_7$), sodium borohydrate ($NaBH_4$), and hydrogen peroxide (H_2O_2), bovine serum albumin (BSA), IgG, myoglobin, haptoglobin, citrulline, fibrinogens were purchased from Sigma-Aldrich (USA). The CXCL5 ELISA kit was purchased from R & D Systems (USA) and was used as per the manufacturer instructions. Phosphate buffer (desired pH) was prepared using monobasic and dibasic sodium phosphates following general laboratory procedure. All other chemicals were of extra pure analytical grade and were used without further purification. Human breast adenocarcinoma (SK-BR3), cervical cancer (HeLa), human colorectal cancer (HT-29) cell lines were obtained from American Type Culture Collection. Dulbecco's Modified Eagle's Medium (DMEM) was purchased from BioWhittaker®, whereas RPMI-1640 medium, fetal bovine serum (FBS) and other cell culture materials including Dulbecco's phosphate buffered saline (PBS) were purchased from Sigma® (USA)

2.2. Apparatus

All electrochemical experiments were done in a conventional three electrode cell system using a potentiostat/galvanostat, Kosentech, model KST P-2 (South Korea). The modified glassy carbon electrode (GCE) (dia. 3.0 mm), Ag/AgCl (in saturated KCl), and a platinum (Pt) wire were used as working, reference, and counter electrodes, respectively. The QCM experiment was performed using a SEIKO EG & G model QCA 917 and a PAR model 263 A potentiostat/galvanostat (USA). An Au-coated working electrode (area: 0.196 cm^2; 9 MHz; AT-cut quartz crystal) was used to perform the quartz crystal microbalance (QCM) experiment in a noise free cabinet. The impedance spectra were obtained at an open circuit voltage between 100 Hz and 1 MHz and a sampling rate of five points per decade using an EG & G Princeton Applied Research PARSTAT2263. X-ray photoelectron spectroscopy (XPS) was performed using a VG Scientific XPSLAB 250 XPS spectrometer and a monochromated Al Kα source with charge compensation at KBSI (Busan). The scanning electron microscopy (SEM) images were obtained using a Cambridge Stereoscan 240 at KBSI (Busan).

2.3. Biosensor fabrication

The diagram of bifunctional nanobiosensor for (i) chemokine ligand selection and (ii) CXCL5 detection has been shown in Scheme 1. In the first step, AuNPs were electrodeposited onto the GCE before the polymerization of TBA in a 0.5 M H_2SO_4 solution containing 0.001%

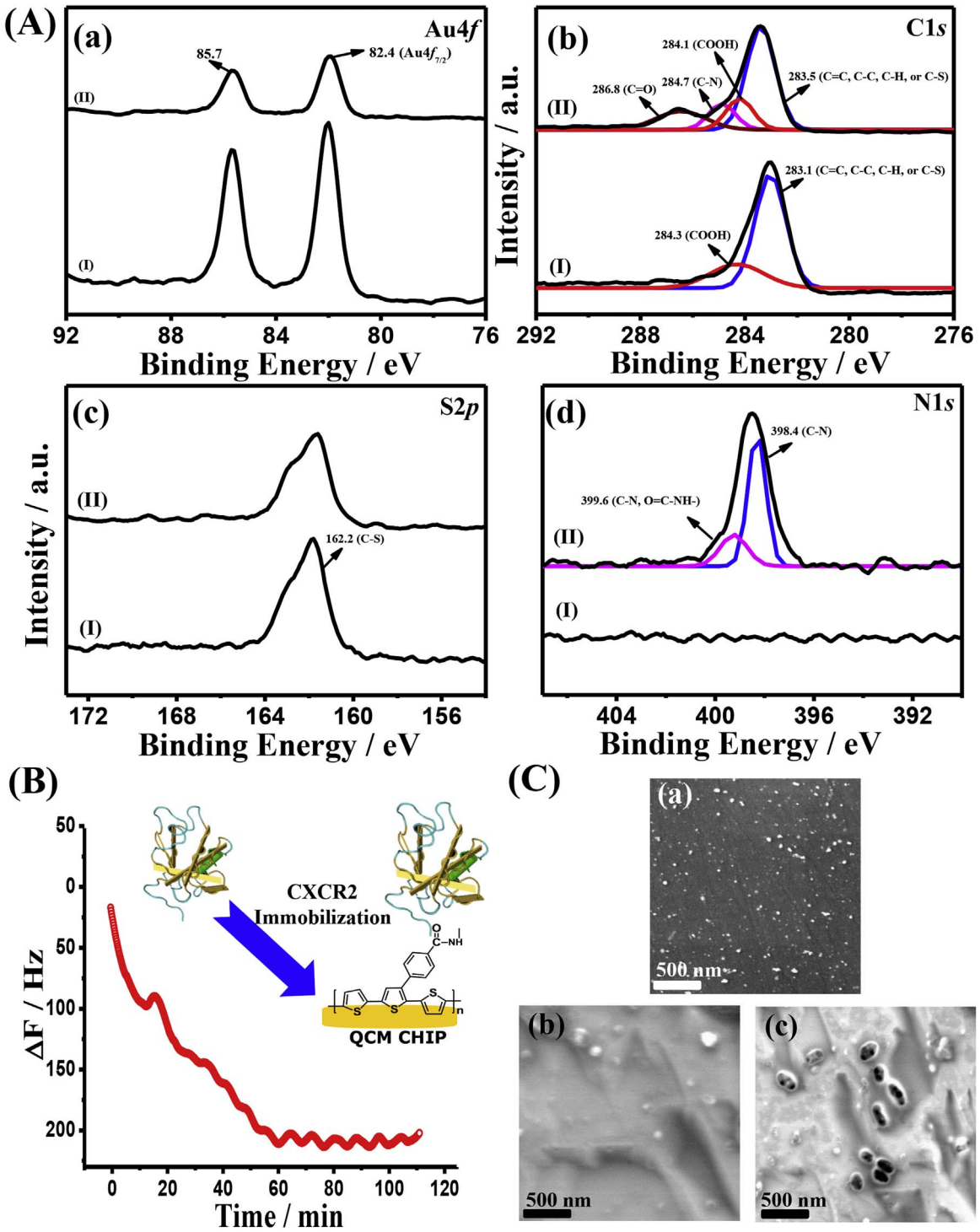

Fig. 1. (A) XPS spectra of (I) GCE/AuNPs/pTBA and (II) GCE/AuNPs/pTBA/CXCR2 surface for (a) Au4f, (b) C1s, (c) S2p, and (d) N1s. (B) Frequency change during the immobilization of CXCR2 on the pTBA surface. (C) SEM images of (a) GCE/AuNPs, (b) GCE/AuNPs/pTBA, and (c) GCE/AuNPs/pTBA/CXCR2.

$HAuClO_4$ using linear sweep voltammetry (LSV) from +1.5 to +0.4 V using the electrodeposition conditions as follows: 60.0 s deposition time, − 0.6 V deposition potential, 0.1 V s^{-1} scan rate, and potential scanning three times (optimized). The pTBA layer was formed on the GCE/AuNPs through electropolymerization of 1.0 mM TBA monomer in a 0.1 M TBAP/CH_2Cl_2 solution by three-time potential cycling between 0.0 and + 1.4 V at scan rate of 0.1 V s^{-1} (optimized). After polymerization, the carboxylic acid groups of the pTBA layer were activated with EDC/NHS and CXCR2 was immobilized to the GCE/AuNPs/pTBA to form the GCE/AuNPs/pTBA/CXCR2 sensing probe. Next, the colloidal AuNPs were formed on the GCE/AuNPs/pTBA/CXCR2 sensor probe surface to make the electrode surface more conducting. In the final step, the electrode was dipped with 0.1% of BSA to block the unbound binding sites to eliminate false positive results. The formation of each layer was examined by XPS and SEM and the real-time CXCR2 immobilization was quantitatively analyzed by QCM.

2.4. Biocompatibility analysis of sensor surface using cytotoxicity assay

CXCL5 concentrations have been eventually analyzed in colorectal

cancer cells samples, which provide information about the role of CXCL5 in cancer cells proliferation, migration, therapeutic intervention, *etc*. Therefore, biocompatibility study of the sensing probe is extremely critical in clinical diagnosis and therapeutics. The cytotoxicity of the sensor surface was assessed by growing mammalian cells in the presence of functionalized probe surface (FPS) (AuNP-TBA composite) material dispersed in microtiter well plate. MTT [3-(4,5-dimethylthiazol-2-yl)-2,5-diphenyltetrazolium bromide] assay was performed to confirm the biocompatibility which depends on the transformation of a tetrazolium compound (MTT) to purple colored formazan crystals due to the activity of mitochondrial dehydrogenase present in cells (Srivastava et al., 2015). To do this, SK-BR3 and HeLa cells were cultured separately in T-75 tissue culture flasks (Nunc, Denmark) at 37 °C in a 5% CO_2 humidified incubator in appropriate media with supplements. Cells were seeded in distinct wells containing 100 µL medium at a final density of 3×10^5 cells/well in a 96 well microtiter plates under the similar experimental conditions. After overnight incubation, the cells were treated with FPS, dimethyl sulfoxide (DMSO) (carrier solvent) as (-) control, and anticancer drug treated as (+) control in separate experiments. All the treated cell samples were incubated at 37 °C in a 5% CO_2 and were performed in triplicate. After 18 h of incubation, 10 µL of MTT reagent (5 mg/mL) was added to each well and the plate was incubated at 37 °C in the dark for 4 h. After this, the media along with MTT was washed off and the formazan crystals were solubilized in DMSO (100 µL/well). The reduction of MTT was analyzed by measuring the absorbance at 570 nm by using a microplate reader. The effect of FPS on cell viability was calculated using Eq. (1):

$$\%Cell\ viability = [(OD_{570}\ of\ FPS\ treated\ cells)/(OD_{570}\ of\ untreated\ cells)] \times 100 \quad (1)$$

3. Results and discussion

3.1. Characterization and morphology of sensor probe

At first, the AuNPs were electrodeposited onto the GCE using LSV where the reduction peak current increased with an increase in the number of sweep which clearly shows the successful deposition of AuNPs and increase in the conductivity of GCE surface (figure not shown). The results obtained for the AuNPs electrodeposition were comparable with our previously reported result (Chandra et al., 2013). In the next step, the pTBA film was formed on the GCE/AuNPs surface by electropolymerization from a 1.0 mM TBA monomer solution. During the anodic scan from 0.0 to + 1.4 V in a 1.0 mM TBA solution, the monomer oxidation peak appeared at + 1.2 V. It had a small reduction peak appeared at + 0.75 V in the reverse cathodic scan from + 1.4 V, corresponding to the reduction of the oxidized polymer film formed on the electrode surface. Larger redox peak currents were obtained here compared to those from polymerization without AuNPs (figure not shown). This was due to the increase in the conductivity of the polymer layer, eventually assisting in the development of highly sensitive sensing probe.

To further confirm the biosensor fabrication, the modification steps were evaluated employing XPS, SEM, and QCM. Firstly, each layer of the biosensor probe was analyzed using XPS, which were recorded after 50 s of Ar ion gas etching and standardized with a C1s peak at 284.6 eV as an internal standard. Fig. 1(A) shows the deconvoluted XPS spectra of (a) Au4f, (b) C1s, (c) S2p, and (d) N1s. The Au4f spectrum of GCE/AuNPs/pTBA shows two clear peaks at 85.7 and 82.4 eV, which appears due to the successful AuNPs deposition (Fig. 1A(a)). The C1s spectrum for pTBA surface shows two distinct peaks at 283.1 and 284.3 eV that are related to the C=C, C–C, C–H, or C–S bonds, and C=O, C–O bonds, respectively (Fig. 1A(b)). After immobilization of the CXCR2 (GCE/AuNPs/pTBA/CXCR2), a new peak C-N at 284.7 eV appeared due to the bond formation between - COOH groups of pTBA and - NH_2 groups of CXCR2, while the peak corresponding to C=O bond was shifted toward the high energy at 286.8 eV. The pTBA layer shows S2p peak at 162.2 eV corresponding to the C–S bond, which was due to the sulfur component of pTBA (Fig. 1A(c)), while the peak at 162.2 eV was not observed for the GCE/AuNPs surface (not shown). This result clearly indicates the successful preparation of AuNPs-pTBA composite. Furthermore, when we examined the deconvoluted N1s spectrum of GCE/AuNPs/pTBA/CXCR2 surface, clear peaks at 398.4 and 399.6 eV were observed which corresponded to the C–N, –C=O–NH- bonds formation due to the covalent bond formation between - NH_2 groups of CXCR2 and - COOH groups of pTBA, indicating successful CXCR2 immobilization (Fig. 1A(d)). No such peaks were observed in the N1s spectrum for the GCE/AuNPs/pTBA surface, indicating that these peaks were merely due to the CXCR2 immobilization. This result also shows the importance of pTBA towards CXCR2 immobilization by covalent bonding formation, which may eventually offer a stable biosensor.

We also studied the CXCR2 immobilization time onto the pTBA surface using and QCM, where the amount of CXCR2 was estimated based on the frequency change (Fig. 1(B)). During CXCR2 immobilization, a decay in the frequency reaches a stable state after 60.0 ± 4.0 min with an overall frequency change (Δf) of 194 ± 13 Hz, corresponding to a mass change (Δm) of 213.18 ± 22.8 ng using Eq. (2).

$$\Delta m = \Delta f \times 5.608(\mathrm{ng/cm^2})/\mathrm{Hz} \times 0.196\mathrm{cm^2} \quad (2)$$

where, Δf was the change in frequency, 5.608 (ng/cm^2)/Hz was the sensitivity factor calculated from the physical constant for quartz, and 0.196 cm^2 was the electrode area. The control experiment in a blank buffer solution (without CXCR2) was also performed, where no decrease in the frequency was observed indicating that the change in the frequency in the earlier case was purely due to CXCR2 immobilization.

We also observed the surface morphology of the sensor probe using SEM (Fig. 1(C)). The SEM image of the GCE/AuNPs layer (Fig. 1C(a)) shows the presence of AuNPs with the particle size of 20.0 ± 1.5 nm, whereas the GCE/AuNPs/pTBA (Fig. 1C(b)) displays a thin film of pTBA over the electrodeposited AuNPs. After immobilization (Fig. 1C(c)), the surface morphology of the sensor was changed and the aggregated structure was observed, due to the immobilization of CXCR2.

3.2. Cytotoxicity analysis of the sensing probe and CXCR2 – chemokines interaction study

The biocompatibility of the sensing probe was analyzed by MTT assay using SK-BR3 and Hela cells (Fig. 2). The % viability was 89 ± 7%

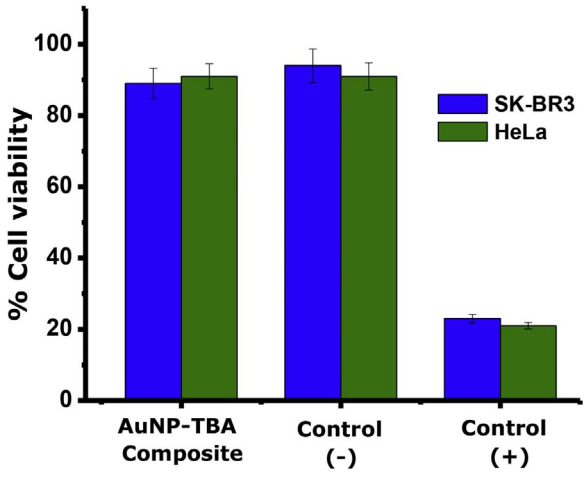

Fig. 2. Biocompatibility evaluation of the sensor probe surface using MTT assay. Error bar shows the mean ± SD of three individual observations.

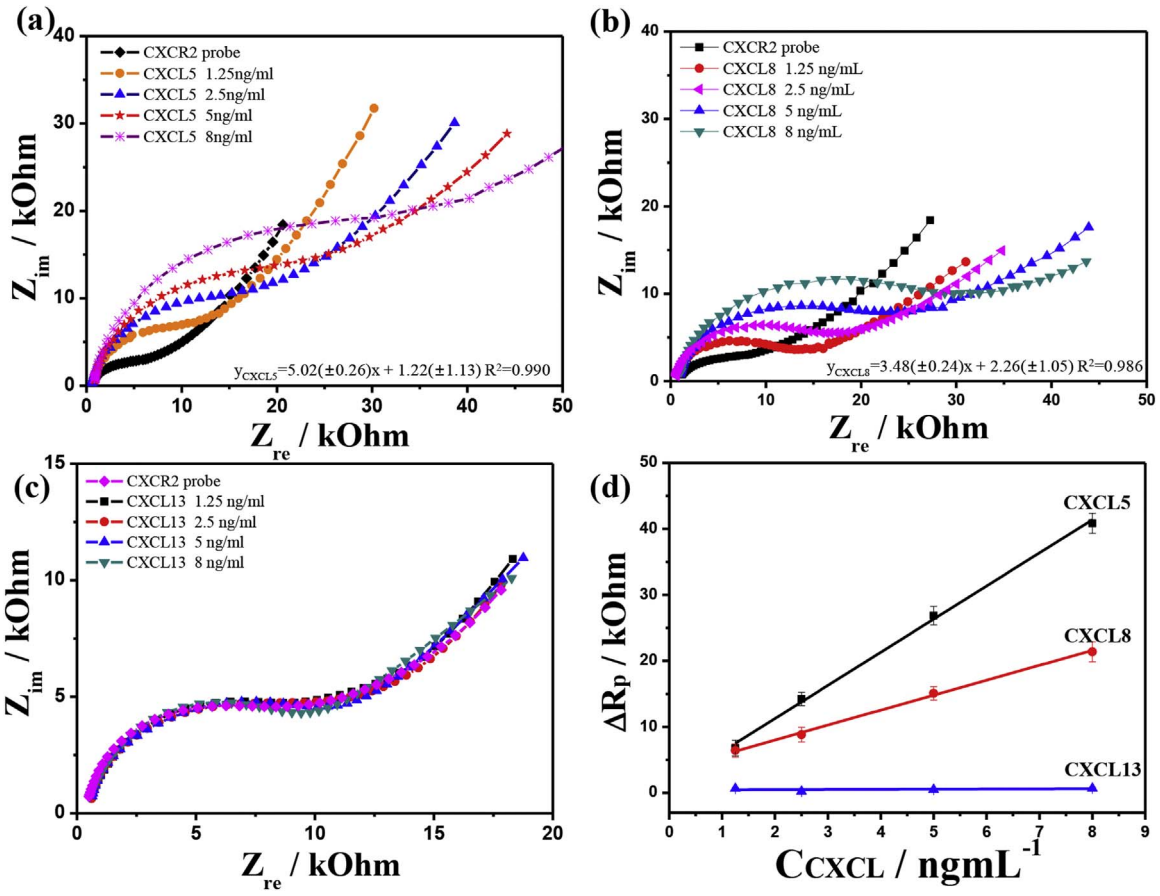

Fig. 3. EIS signals recorded after (a) CXCL5, (b) CXCL8, (c) CXCL13 interaction with the GCE/AuNPs/pTBA/CXCR2 sensor probe in a 0.1 M PBS (pH 7.4) and (d) linear plots showing the dose dependent responses of CXCL5, CXCL8, and CXCL13 interaction with the sensor probe. Error bar shows the mean ± SD of three individual observations.

and 91 ± 5% ($n = 3$) for SK-BR3 and Hela cells, respectively, indicating that the sensor probe materials don't exert any toxic effect. This result was further confirmed by performing positive and negative control experiments. Cells treated with DMSO (negative control) and daunomycin (10 μg/mL) (positive control), interestingly showed the cell viability of 97 ± 6% and 20 ± 1%, respectively for both the cell lines. These experiments confirm that the sensing probe used in the present study is biocompatible and can be further use for the biomedical analysis using *in vitro* and *in vivo* models.

In the subsequent step, the interaction between chemokines and CXCR2 sensor probe was studied to find out the best ligand using EIS. For this purpose, CXCL5, CXCL8, and CXCL13 were allowed to interact for 30 min with the GCE/AuNPs/pTBA/CXCR2 sensor probe in separate experiments. After washing with PBS three times, EIS spectra in the Nyquist plot was recorded in 0.1 M PBS. Fig. 3 shows the EIS spectra for (a) CXCL5, (b) CXCL8, and (c) CXCL13 interaction with the GCE/AuNPs/pTBA/CXCR2 sensor probe, where the Rct value increased significantly for CXCL5 followed by CXCL8. In case of CXCL13, negligible increase in the Rct value was observed indicating that the sensor probe doesn't interact with CXCL13. A comparative study of dose dependent interaction between 1.25 and 8.0 ng/mL concentrations is shown in Fig. 3(d), where the slope of the calibration plot was significantly higher for CXCL5 (5.02 (± 0.26)) compared to CXCL8 (3.48 (± 0.24)). The comparison was also found statistically significant with $p < 0.0001$, which clearly shows that CXCL5 interacted with the designed sensor probe with the highest affinity.

3.3. Optimization of experimental parameters

The analytical parameters for the detection of CXCL5 using the biosensor were optimized in terms of CXCR2 concentration, temperature, pH, and incubation time, where CXCL5 concentration was kept constant (Fig. S1). The effect of CXCR2 concentration was studied between 1 and 50 μg/mL. The response signal gradually increased from 1 to 30 μg/mL, however, it did not increase over 30 μg/mL, possibly due to the saturation of the active sites for CXCR2 immobilization (Fig. S1(A)). Thus, 30 μg/mL CXCR2 concentration was used in the subsequent experiments. The effect of temperature on the CXCR2–CXCL5 interaction was studied between 10 and 50 °C. The signal increased as the temperature increased from 10 to 35 °C (Fig. S1(B)). From 35–40 °C the signal was almost similar, but over 40 °C the signal slightly decreased, whereas it decreased significantly at increased temperature due to denaturation of CXCR2 and/or CXCL5. Based on the temperature response, an optimum value of 35 °C was selected for further experiments. The optimized temperature is practically comparable to the human body fluids allowing the potential application of the biosensor in real sample analysis from hospitals. The effect of pH on the CXCR2–CXCL5 interaction was studied over a range of 5–8. The response current increased from pH 5 to pH 7.5, but the current did not increase significantly above pH 7.5. Thus, pH 7.5 was used in further experiments (Fig. S1(C)). The optimized pH is near to the physiological pH of various body fluids enabling its practical application to detect CXCL5 in real body fluids. The effect of incubation time for the ligand - receptor interaction was optimized by dipping the sensor probe with CXCL5 for different lengths of time ranging from 1 to 30 min. The signal increased as the reaction time went from 1 to 20 min, but no significant increase in the signal was observed over 20 min, possibly due to the saturation effect, where all the active sites were occupied by CXCR2 (Fig. S1(D)). Thus, 20 min incubation time was applied for further experiments.

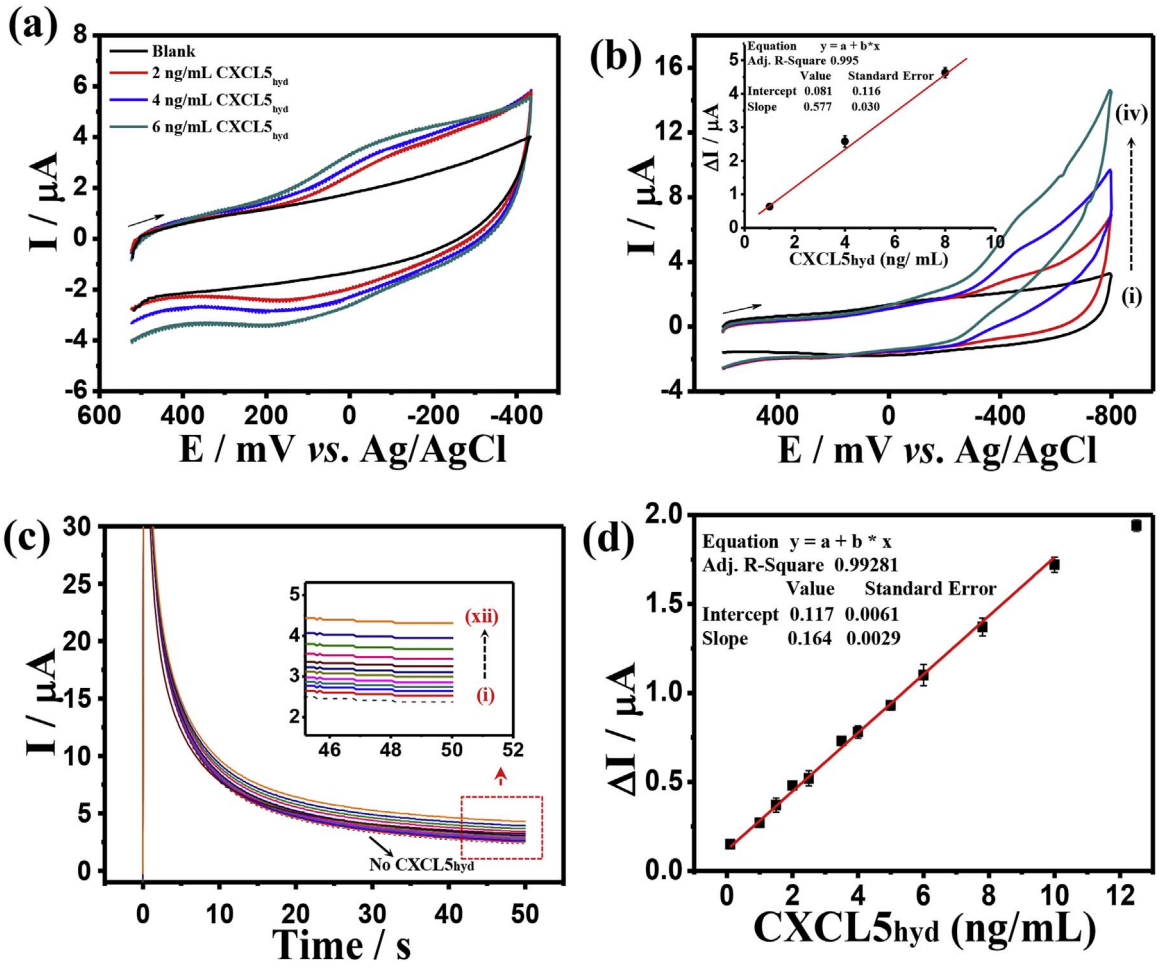

Fig. 4. (a) CVs of GCE/AuNPs/pTBA/CXCR2 sensor probe for various concentrations of $CXCL5_{Hyd}$, (b) CVs of GCE/AuNPs/pTBA/CXCR2/$CXCL5_{Hyd}$ probe for increasing $CXCL5_{Hyd}$ concentrations in 0.1 M PBS containing 4.0 mM H_2O_2: inset shows the linear plot between 1 and 8 ng/mL $CXCL5_{Hyd}$ concentrations, (c) chronoamperometric responses for the $CXCL5_{Hyd}$ detection using the sensor probe in deoxygenated PBS containing 4.0 mM H_2O_2 (pH 7.4), applied potential: − 450 mV *vs.* Ag/ AgCl, inset: magnified chronoamperometric signal from 46 to 50 s, (d) calibration plot based on the signals obtained in the chronoamperometric responses for $CXCL5_{Hyd}$ detection.

3.4. Detection of CXCL5 and analytical performance of biosensor

At first, we established the ability of the biosensor to detect CXCL5 in dose dependent manner using voltammetry. For this purpose, firstly a facile pretreatment step was performed where CXCL5 was linked with hydrazine (hyd) following an earlier reported method (Kim et al., 2009). Thereafter, hyd-linked CXCL5 ($CXCL5_{hyd}$) was incubated with the sensor probe. After washing with the PBS, CV was recorded by cycling the potential between + 500 and − 400 mV at a scan rate of 50.0 mV s^{-1} in a deoxygenated PBS. Interestingly, a redox peak at −90/140 mV was observed due to the direct electron transfer behavior of hyd itself which linearly increased with $CXCL5_{hyd}$ concentrations from 2 to 6 ng/mL as shown in Fig. 4(a). To ensure the stability of this complexation reaction, CVs were recorded at the scan rates between 20 and 100 mV s^{-1}. The peak currents in the CVs were directly proportional to the scan rates, indicating a surface - confined electrochemical process (Moon et al., 2017). This clearly shows that $CXCL5_{hyd}$ is effectively captured by the CXCR2 sensor probe. No signal, however, was observed when $CXCL5_{hyd}$ reacted with CXCR2 unimmobilized probe (GCE/AuNPs/pTBA), otherwise indicating that signals in earlier case were merely due to the interaction between CXCR2 sensor probe and $CXCL5_{hyd}$.

The analytical performance of the biosensor was performed under the optimized experimental conditions. Firstly, the GCE/AuNPs/pTBA/CXCR2/$CXCL5_{hyd}$ probe was dipped in PBS containing 4.0 mM H_2O_2 followed by cycling the potential between + 0.3 and − 0.8 V at a scan rate of 50.0 mV s^{-1}. Interestingly, a clear reduction peak at approximately − 430 mV was observed due to the catalytic reduction of H_2O_2 by $CXCL5_{hyd}$ (Fig. 4(b)), which increased with $CXCL5_{hyd}$ concentrations between 1 and 8 ng/mL (inset of Fig. 4(b)). On the other hand, no catalytic peak was observed when CXCL5 without hyd labeling was allowed to react with the GCE/AuNPs/pTBA surface (black curve (i) of Fig. 4(b)), indicating that the signal in the earlier case was merely due to the interaction between the receptor and the ligand. Fig. 4(c) shows the chronoamperometric responses of the developed biosensor at − 450 mV *vs.* Ag/AgCl (optimized) in deoxygenated PBS containing 4.0 mM H_2O_2 after interacting with different concentrations of $CXCL5_{hyd}$. Chronoamperometric results clearly show increase in the current responses with increase in the $CXCL5_{hyd}$ concentrations, indicating that the target molecule is effectively detected by the developed biosensor (Fig. 4(c)). Based on the result, a calibration plot was obtained, which showed a linear response for $CXCL5_{hyd}$ detection ranging from 0.1 to 10 ng/mL (Fig. 4(d)). The linear regression equation of the calibration plot was expressed as follows: ΔI (μA) = 0.117 (± 0.0061) + 0.164 (± 0.0029) [$CXCL5_{hyd}$] with the correlation coefficient of 0.992. The detection limit of CXCL5 was determined to be 0.078 ± 0.004 ng/mL (RSD < 4.7%) based on the standard deviation of five repeated measurements of the blank (95% confidence level, $n = 5$). Importantly, the detection range obtained in this case falls at the serum CXCL5 concentrations of patients suffering from nasopharyngeal carcinoma (0.135 − 3.058 ng/mL) (Zhang et al., 2013) and colorectal cancer (0.20–5.71 ng/mL) (Kawamura et al., 2012), indicating the

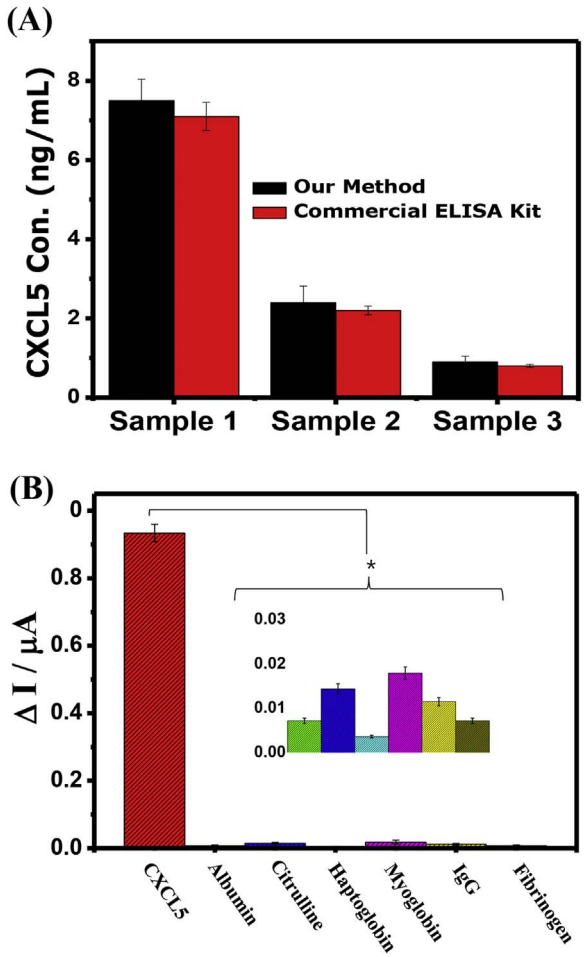

Fig. 5. (A) Histogram showing detection of CXCL5 using the sensor probe and commercially available ELISA Kit. (B) Histogram showing the selective detection of CXCL5 using the sensor probe at 5 ng/mL concentration.

immense clinical importance of our results. A Table S1 shows the analytical performance of various analytical methods for chemokines detection. We also validated our biosensing results with a commercially available ELISA kit, where three independent samples were analyzed. The CXCL5 levels detected using both methods were comparable with each other at the 95% confidence level ($n = 9$), indicating the accuracy of our method (Fig. 5(A)).

3.5. Selectivity, reproducibility, and stability

Selectivity of the proposed sensor was demonstrated by testing the compounds that are majorly present in the real sample matrix, such as albumin, citrulline, haptoglobin, myoglobin, IgG, and fibrinogens. All experiments were performed for 1, 5, and 10 ng/mL concentrations. Fig. 5(B) shows the responses of interfering molecules along with CXCL5, where the negligible signal is observed for the interfering molecules compared to CXCL5 (data shown only for 5 ng/mL). This result also suggests that these molecules don't interact with the sensing surface, hence not occupying the CXCL5 binding sites. The selectivity obtained was due to CXCR2 immobilized on the nanocomposite film, which doesn't interact with other nontarget molecules. The selectivity results were also statistically significant showing $p < 0.0001$. We also tested the ability of the biosensor to detect target CXCL5 in presence of the interfering molecules in a mixed sample solution. Interestingly, the sensitivity of the detection in this case was 93 ± 2% ($n = 5$) compared when CXCL5 was detected alone, indicating its selective detection in a mixed sample solution. The reproducibility of the biosensor was evaluated which show the RSD < 4.7% ($n = 5$) and the electrode-to-electrode RSD was < 5.3% even when the same fabrication steps were followed. This small deviation was probably due to the minor variation in the sensor fabrication. We also examined the long-term stability of the sensor with respect to time, where the sensor retained almost 95 ± 3% of its sensitivity upto six weeks. The response decreased about 8 ± 1% after six weeks and then further decreased with time. Thus, the sensor was reasonably stable up to six weeks. The good stability was due to the stable covalent attachment of the CXCR2 on the conducting polymer-nanoparticle composite, which maintained its biological activity.

3.6. Real sample analysis using human serum and colorectal cancer cells

Since CXCL5 concentrations in a serum sample provides the prognostic index of cancer (Kawamura et al., 2012), we selected serum as a matrix for real sample analysis. Known concentrations of $CXCL5_{hyd}$ were spiked in the undiluted human serum samples in the dynamic range between 0.1 and 10 ng/mL. The % recovery of $CXCL5_{hyd}$ from the human serum samples were quantified using Eq. (3).

$$(\%)\text{Recovery} = \frac{a_{sp} - a_b}{a_s} \times 100 \quad (3)$$

where a_{sp} and a_b are the analytical response of $CXCL5_{hyd}$ in the spiked and blank samples, respectively; a_s is the analytical response of $CXCL5_{hyd}$ in the standard solutions

The response in serum samples were 94 ± 2% in this case, indicating that the biosensor can effectively detect CXCL5 in real sample matrix within 25 min, hence it is robust and extremely valuable for direct clinical applications. The linear regression equation for the calibration plot in the serum sample was expressed as follows: $\Delta I\ (\mu A) = 0.098\ (\pm 0.009) + 0.113\ (\pm 0.007)\ [CXCL5_{hyd}]$ with the correlation coefficient of 0.914. The detection limit of CXCL5 in serum sample was determined to be 0.085 ± 0.007 ng/mL (RSD < 6.3%) based on the standard deviation of five repeated measurements of the blank (95% confidence level, $n = 5$).

We also investigated the *in vitro* diagnostic ability of the biosensor for CXCL5 detection in colorectal cancer cell (HT-29 cells) samples since they are known to secrete CXCL5 extracellularly (Ashton Acton, 2013). In this experiment, we spiked 2.5, 5.0, and 7.5 ng/mL of $CXCL5_{hyd}$ in the autoclaved PBS solution containing the 10^5 cells/mL. The response of $CXCL5_{hyd}$ was analyzed using the fabricated sensor which was found to be 93 ± 3% with reference to the values obtained in the blank buffer solution (RSD < 5.3%, $n = 5$). These results clearly show the ability of the sensor to detect CXCL5 in colorectal cancer cells samples which is considered to be a most relevant *in vitro* model to study cancer prognosis based on extracellular CXCL5 detection (Kawamura et al., 2012; Kowalczuk et al., 2014). The linear regression equation of the calibration plot for the cell sample analysis is expressed as follows: $\Delta I\ (\mu A) = 0.0978\ (\pm 0.0091) + 0.112\ (\pm 0.0081)\ [CXCL5_{hyd}]$ with the correlation coefficient of 0.912. The detection limit of CXCL5 in colorectal cancer cells sample was determined to be 0.079 ± 0.009 ng/mL (RSD < 5.1%) based on the standard deviation of five repeated measurements of the blank (95% confidence level, $n = 5$)

4. Conclusion

A biocompatible bifunctional nanobiosensor has been successfully developed for the first time to study the interaction between CXCR2 and chemokines. Experimentally, it has been shown that CXCL5 ligand interacts with the CXCR2 receptor with highest affinity, which can be further utilized for various therapeutic strategies. Highly sensitive and selective detection of CXCL5 was achieved by the AuNP-conducting polymer matrix and CXCR2 receptor. A linear relationship for CXCL5 detection was observed between 0.1 and 10 ng/mL, with the detection limit of 0.078 ± 0.004 ng/mL (RSD < 4.1%). The proposed biosensor

was able to detect the CXCL5 directly in human serum samples and colorectal cancer cell model within 25 min unlike the traditional ELISA technique which require several hours. Therefore, the developed method can be applied as a fast routine laboratory test for CXCL5 detection in cell culture supernatant, serum, plasma obtained from clinical laboratories. In future, the sensor prototype can be translated as a point-of-care medical device for various medical applications.

Acknowledgement

This work was supported by the National Research Foundation of Korea (NRF) grant funded by the Korea government (MSIP) (No.2015R1A2A1A13027762). Pranjal Chandra acknowledge support by DST Ramanujan Fellowship (SB/S2/RJN-042/2015), Government of India for completion of this work and IIT Guwahati for providing leave to visit PNU, South Korea.

Appendix A. Supplementary material

Supplementary data associated with this article can be found in the online version at http://dx.doi.org/10.1016/j.bios.2017.09.031.

References

Agarwal, M., He, C., Siddiqui, J., Wei, J., Macoska, J.A., 2013. Prostate 73, 573–581.
Ashton Acton, Q., 2013. Colon Cancer: New Insights for the Healthcare Professional. Scholarly Editions, Gorgia.
Balkwill, F., 2004. Nat. Rev. Cancer 4, 540–550.
Bardea, A., Patolsky, F., Dagan, A., Willner, I., 1999. Chem. Commun. 21–22.
Ben-Baruch, A., 2012. The Inflammatory Milieu of Tumors: Cytokines and Chemokines that Affect Tumor Growth and Metastasis. Bentham Science Publishers.
Bersini, S., Jeon, J.S., Dubini, G., Arrigoni, C., Chung, S., Charest, J.L., Moretti, M., Kamm, R.D., 2014. Biomaterials 35, 2454–2461.
Chandra, P., Noh, H.-B., Won, M.-S., Shim, Y.-B., 2011. Biosens. Bioelectron. 26, 4442–4449.
Chandra, P., Noh, H.-B., Shim, Y.-B., 2013. Chem. Commun. 49, 1900–1902.
Chandra, P., Noh, H.-B., Pallela, R., Shim, Y.-B., 2015. Biosens. Bioelectron. 70, 418–425.
Chandra, P., 2016. Nanobiosensors for Personalized and Onsite Biomedical diagnosis. The Institution of Engineering and Technology, London (UK).
Cyster, J.G., 1999. Science 286, 2098–2102.
Hussain, K.K., Moon, J.-M., Park, D.-S., Shim, Y.-B., 2017. Electroanalysis 29. http://dx.doi.org/10.1002/elan.201700308.
Kawamura, M., Toiyama, Y., Tanaka, K., Saigusa, S., Okugawa, Y., Hiro, J., Uchida, K., Mohri, Y., Inoue, Y., Kusunoki, M., 2012. Eur. J. Cancer 48, 2244–2251.
Kim, D.-M., Noh, H.-B., Park, D.S., Ryu, S.-H., Koo, J.S., Shim, Y.-B., 2009. Biosens. Bioelectron. 25, 456–462.
Kim, D.-M., Shim, Y.-B., 2013. Biosens. Bioelectron. 85, 6536–6543.
Kowalczuk, O., Burzykowski, T., Niklinska, W.E., Kozlowski, M., Chyczewski, L., Niklinski, J., 2014. Tumour Biol. 35, 4619–4628.
Koh, W.C.A., Chandra, P., Kim, D.-M., Shim, Y.-B., 2011. Anal. Chem. 83, 6177–6183.
Kwon, N.H., Rahman, M.A., Won, M.-S., Shim, Y.-B., 2006. Anal. Chem. 78, 52–60.
Le, Y., Zhou, Y., Iribarren, P., Wang, J.M., 2004. Cell. Mol. Immunol. 1, 95–104.
Lee, T.-Y., Shim, Y.-B., 2001. Anal. Chem. 73, 5629–5632.
Li, A., King, J., Moro, A., Sugi, M.D., Dawson, D.W., Kaplan, J., Li, G., Lu, X., Strieter, R.M., Burdick, M., Go, V.L.W., Reber, H.A., Eibl, G., Hines, O.J., 2011. Am. J. Pathol. 178, 1340–1349.
Moon, J.-M., Kim, D.-M., Kim, M.H., Han, J.-Y., Jung, D.-K., Shim, Y.-B., 2017. Biosens. Bioelectron. 91, 128–135.
Rahman, M.A., Park, D.S., Won, M.-S., Park, S.-M., Shim, Y.-B., 2004. Electroanalysis 16, 1366–1370.
Rahman, M.A., Kumar, P., Park, D.-S., Shim, Y.-B., 2008. Sensors 8, 118–141.
Srivastava, A., Aggarwal, L., Jain, N., 2015. ACS Comb. Sci. 17, 39–48.
Sun, H., Chung, W.-C., Ryu, S.-H., Ju, Z., Tran, H.T., Kim, E., Kurie, J.M., Koo, J.S., 2008. Cancer Prev. Res (Phila.). 1, 316–328.
Thomson, W., Lotze, M.T., 2003. The Cytokine Handbook, fourth ed. Elsevier Science Publishing Company, San Diego.
Zhang, H., Xia, W., Lu, X., Sun, R., Wang, L., Zheng, L., Ye, Y., Bao, Y., Xiang, Y., Guo, X., 2013. PLoS One 8, e57830.
Zhu, Y., Chandra, P., Song, K.-M., Ban, C., Shim, Y.-B., 2012. Biosens. Bioelectron. 36, 29–34.